

THE SIMULATION AND PERFORMANCE OF A CENTRIFUGAL CHILLER

W.L. Jackson

F.C. Chen, P.E.

B.C. Hwang, Ph.D.

ABSTRACT

A computer simulation model was developed to analyze the performance of a water-cooled centrifugal chiller. The model is based on a heat pump thermodynamic cycle and empirical correlations for the performance of the system components. The system simulated is composed of a variable-speed centrifugal compressor with a hot-gas bypass option for capacity control, two shell-and-tube heat exchangers, and an expansion device. The model was validated and calibrated against the experimental test results of a 125-ton chiller. The performance of a similar chiller system at various operating conditions and design modifications was analyzed. System performance comparisons were made between a baseline case, cases with high-performance heat exchanger tubes and compressor motor, and various variable-speed compressor operating strategies. It was found that significant performance improvement can be realized by using variable-speed drive and an on-demand control strategy.

INTRODUCTION

Centrifugal chillers are often used to meet large-scale air-conditioning or cooling needs in commercial buildings, shipboard, and industrial applications. In the U.S. commercial sector alone, more than 40% of the total commercial air-conditioning equipment capacity is provided by centrifugal chillers (TRW 1982). While the number of centrifugal chiller units is far less than that of residential air conditioners, their total resource energy consumption is nevertheless substantial.

Several computer simulation models (Freeman et al. 1975; Hiller and Glicksman 1976; Flower 1978; Ellison and Creswick 1978; Fischer and Rice 1983; and Domanski and Didion 1983) have been developed to study residential air conditioners and heat pumps for design and performance improvements. The Freeman et al. (1985) model was used to compare solar systems with air-to-air systems for residential applications. The Domanski and Didion (1983) model contained detailed reciprocating compressor, capillary tube, and air-to-air heat exchanger models. Ellison and Creswick (1978) combined the trio of Hiller and Glicksman models (1976) and introduced more user-convenient reciprocating compressor and flow expansion device subroutines. This residential, air-to-air heat pump computer model was further developed into a computer-aided design tool for performance improvement studies (Rice et al. 1981) by including two types of reciprocating compressor representations, more flow expansion devices, and a variety of air-to-refrigerant heat exchanger geometry options (Fischer and Rice 1983). Oliver, Sepsy, and Jones (1973) analyzed a commercial-sized air-conditioning system using reciprocating compressors. Computer simulations for performance improvement of centrifugal

W. L. Jackson is a member of the Computing and Telecommunications Division, Oak Ridge National Laboratory, Oak Ridge, TN. F. C. Chen is a member of the Efficiency and Renewables Research Section, Energy Division, Oak Ridge National Laboratory, Oak Ridge, TN. B. C. Hwang is a project manager at the David Taylor Naval Ship R&D Center, Annapolis, MD.

chillers are scarce. All of the above models used reciprocating compressors and refrigerant-to-air heat exchangers. Thus, none of them were suited for the centrifugal chiller system with refrigerant-to-water heat exchangers presented in this paper. The development of a computer model for centrifugal chillers with refrigerant-to-water heat exchangers has been discussed by Hwang et al. (1985).

Centrifugal chillers are generally more energy efficient than residential air-conditioning/heat pump units. However, energy saving opportunities for chillers do exist. This paper presents the results of a parametric performance study, carried out through computer simulation of a centrifugal chiller under various design/component variations and operating conditions. Simulation results of a baseline case were validated against actual capacity test data. Two centrifugal chiller design variations were analyzed using seawater as the heat sink for the condenser, and the analytical results are presented.

MODEL DESCRIPTION

Basic Cycle

A schematic of a basic centrifugal chiller with a hot-gas bypass control is shown in Figure 1. The principal components of the system include a motor-driven centrifugal compressor, a shell-and-tube condenser, a shell-and-tube evaporator, and an expansion device. Refrigerant vapor is compressed from a low-temperature, low-pressure state to a higher pressure in the compressor. The resulting refrigerant state is at a much higher temperature. The hot vapor then passes into the condenser where it condenses on heat exchanger tubes, heating the water that flows through the tubes. The hot liquid refrigerant then flows through an expansion valve, dropping to a low-temperature, low-pressure state with a mixture of liquid and vapor, two-phase refrigerant. This cold refrigerant then passes into the evaporator where it boils as it comes in contact with heat exchanger tubes, cooling the water that flows through the tubes. The resulting low-pressure refrigerant vapor then reenters the compressor, starting the cycle again. The motor generates a small amount of heat because of its inefficiency, which is absorbed by passing refrigerant through it, using either (1) the refrigerant vapor leaving the compressor or (2) the refrigerant liquid leaving the condenser.

The hot-gas bypass option is a conventional means for capacity control. When the hot-gas bypass is used, some saturated refrigerant vapor bypasses the condenser and enters the evaporator, resulting in reduced heat transfer rates in the condenser and evaporator. The bypass is necessary to prevent compressor stalling at low capacity.

The heat pump model is based on the heat pump thermodynamic cycle and uses empirical correlations for the performance of the system components. The basic thermodynamic cycle used for the calculations is shown in Figure 2 as a pressure vs. enthalpy diagram in which the calculation points are numbered 1 through 11.

The iterative calculations begin at point 1, the entrance to the compressor. Point 2 represents the exit from the compressor, and, if the motor is cooled by the discharge line, point 3 represents the state of the refrigerant after it has passed over the motor. Point 4 represents the refrigerant state after isentropic compression. Entrance to the condenser at point 4 due to pressure drop in the discharge line, saturated vapor occurs at point 5, and saturated liquid occurs at condenser exit at point 6. With a subcooler, subcooling of the refrigerant may occur between points 6 and 7. Without a subcooler, point 7 will be the same as point 6. Entrance to the expansion device is at point 8 due to pressure drop in the liquid line. If the motor is cooled by the liquid line, point 8 will be at a higher enthalpy than point 7. Entrance to the evaporator is at point 9 and exit is at point 11, which, unless the hot-gas bypass is active, is usually the same as point 10, saturated vapor, because virtually no superheating is expected in a pool boiling evaporator before the vapor reenters the compressor. The hot-gas bypass flow proceeds from point 5 to point 11, mixing with refrigerant in the evaporator.

The compressor suction line is between points 11 and 1, and the discharge line is between points 3 and 4. A liquid line runs between points 7 and 8. Pressure drops are calculated for each of the three refrigerant lines mentioned above. Most of the state point calculations are done by refrigerant properties subroutines based on equations by Downing (1974).

Starting Conditions

An initial guess is made for the condenser and evaporator saturation temperatures. The required refrigerant mass flow rate may be calculated as

$$\dot{m}_R = \dot{Q}_e / (h_{11} - h_9) , \quad (1)$$

where

- h_{11} - refrigerant enthalpy at evaporator exit,
- h_9 - refrigerant enthalpy at evaporator inlet,
- \dot{m}_R - required refrigerant mass flow rate,
- \dot{Q}_e - specified cooling capacity.

Centrifugal Compressor Model

The centrifugal compressor is modeled from a compressor map that was digitized and fitted to a set of bipolynomial equation coefficients. From this map, the compressor flow capacity, \dot{m}_F , and isentropic efficiency, η_s , are determined as functions of the Mach number, M , volumetric flow coefficient, θ , and the head coefficient, Ω :

$$\dot{m}_F = \dot{m}_F(M) , \quad (2)$$

$$\eta_s = \eta_s(\theta, \Omega) , \quad (3)$$

$$\theta = \frac{\dot{m}v_1}{ad^2} , \quad (4)$$

$$\Omega = (h_s - h_1)/a^2 , \quad (5)$$

$$M = \phi \pi d/a , \quad (6)$$

where

- a - sonic velocity at compressor suction,
- d - impeller diameter,
- h_s - refrigerant enthalpy after isentropic compression,
- h_1 - refrigerant enthalpy at compressor suction,
- \dot{m}_F - compressor flow capacity (the refrigerant mass flow rate at full capacity),
- M - Mach number at impeller tips,
- η_s - isentropic efficiency,
- θ - compressor flow coefficient,
- v_1 - refrigerant specific volume at compressor suction,
- π - constant (3.141593),
- ϕ - compressor speed,
- Ω - compressor head coefficient.

The actual refrigerant mass flow rate, \dot{m} , is given by

$$\dot{m} = \text{the smaller of } \dot{m}_R \text{ and } \dot{m}_F \quad (7)$$

If $\dot{m}_R > \dot{m}_F$, the specified cooling capacity cannot be met. The refrigerant enthalpy at the compressor discharge, h_2 , may be calculated by:

$$h_2 = h_1 + (h_s - h_1)/\eta_s , \quad (8)$$

where h_2 is refrigerant enthalpy at compressor discharge. The heat added to the refrigerant after compressor discharge is calculated by

$$h_3 = h_2 + (P_{in} - P_{sh})/\dot{m} \quad (9)$$

$$P_{in} = P_{sh}/\eta_m \quad (10)$$

$$P_{sh} = \dot{m} (h_2 - h_1) \quad (11)$$

where

h_3 = refrigerant enthalpy after passing over the motor,

P_{in} = input power to motor,

P_{sh} = compressor shaft power,

η_m = motor efficiency calculated as a function of P_{sh} .

Shell-and-Tube Condenser and Evaporator Models

The heat exchanger models (shell-and-tube type with refrigerant on the shell side and water inside the tubes) calculate the heat transfer rate, \dot{Q} , based on the log mean temperature difference between the refrigerant and water and an overall heat transfer coefficient that includes a water-fouling coefficient, the conduction coefficient in the tube wall, the water-side heat transfer coefficient for water flowing in the tubes, and a condensing or boiling heat transfer coefficient for the condenser or evaporator, respectively:

$$\dot{Q} = U A_o \text{LMTD} \quad (12)$$

$$U = 1/(H_w^{-1} + H_{foul}^{-1} + H_{wall}^{-1} + H_R^{-1}) \quad (13)$$

$$\text{LMTD} = \frac{T_{w,out} - T_{w,in}}{\ln[(T_{sat} - T_{w,in})/(T_{sat} - T_{w,out})]} \quad (14)$$

where

- A_o = total outside heat transfer area of the heat exchanger,
- H_{foul} = water-fouling heat transfer coefficient (corrected to A_o),
- H_R = refrigerant condensing or boiling heat transfer coefficient for the condenser or evaporator, respectively (based on A_o),
- H_w = water-side heat transfer coefficient (corrected to A_o),
- H_{wall} = tube wall conductive heat transfer coefficient (corrected to A_o),
- LMTD = log mean temperature difference between refrigerant and water,
- ln = natural logarithmic function,
- \dot{Q} = heat transfer rate, based on LMTD, for the condenser or evaporator,
- T_{sat} = refrigerant saturation temperature,
- $T_{w,in}$ = water inlet temperature,
- $T_{w,out}$ = water outlet temperature,
- U = overall heat transfer coefficient.

The water-side heat transfer coefficient, H_w , is based on General Electric Company (1971, 1973), the condensing heat transfer coefficient on correlations from Beatty and Katz (1948), and the boiling heat transfer coefficient from

$$H_R = \lambda \Delta T^\sigma \quad (15)$$

where ΔT is the average temperature difference between tube wall and refrigerant and λ and σ are constants for the boiling heat transfer coefficient. These constants were supplied by the tube manufacturers based on experimental data.

The heat transfer rates, based on the refrigerant states and flow rate, are given by

$$\dot{Q}_e = \dot{m}(h_{11} - h_9) , \quad (16)$$

$$\dot{Q}_c = \dot{m}(h_4 - h_7) , \quad (17)$$

where

- h_4 - refrigerant enthalpy at condenser inlet,
- h_7 - refrigerant enthalpy at condenser exit,
- \dot{Q}_c - heat transfer rate in condenser based on the refrigerant states and flow rate,
- \dot{Q}_e - heat transfer rate in evaporator based on the refrigerant states and flow rate.

An energy balance on the heat exchangers is performed iteratively over the refrigerant saturation temperatures until the heat transfer rate \dot{Q} from Equation 11 equals \dot{Q}_c for the condenser iteration and \dot{Q}_e for the evaporator iteration. An iteration over the compressor and heat exchanger models is necessary to converge on a value for \dot{m} that provides an energy balance in the heat exchanger models at the appropriate T_{sat} values in each heat exchanger.

Hot-Gas Bypass

The hot-gas bypass option is activated in the model if \dot{Q}_e is less than a given value specified in the input data. If the bypass is active, refrigerant vapor, which has been cooled to saturation temperature in the condenser, point 5 in Figure 2, passes from a point in the condenser shell above the liquid pool through the bypass valve and into the evaporator shell.

Refrigerant flow through the hot-gas bypass is regulated by an orifice. The flow through the orifice is assumed to be critical and the refrigerant mass flow rate, \dot{m}_B , is given by

$$\dot{m}_B = k_B (P_5/V_5)^{0.5} , \quad (18)$$

where

- k_B - an empirically derived constant,
- \dot{m}_B - refrigerant mass flow rate in the hot-gas bypass,
- P_5 - refrigerant pressure at point 5,
- V_5 - refrigerant specific volume at point 5.

To maintain the specified cooling capacity, Q_e , based on mass and energy balances in the heat pump system, the required mass flow rate, \dot{m}_R , in Equation 1 is increased by

$$\dot{m}_R = \dot{m} + \dot{m}_B (h_5 - h_9)/(h_{11} - h_9) , \quad (19)$$

where h_5 is the enthalpy of saturated refrigerant vapor in the condenser. Likewise, the evaporator and condenser heat transfer rates, \dot{Q}_e and \dot{Q}_c , in Equations 16 and 17, respectively, are adjusted by

$$\dot{Q}_e = \dot{Q}_e - \dot{m}_B(h_5 - h_9) , \quad (20)$$

$$\dot{Q}_c = \dot{Q}_c - \dot{m}_B(h_5 - h_6) , \quad (21)$$

where h_6 is the refrigerant enthalpy at the condenser exit.

The water-to-water heat pump model (Hwang et al. 1985) was employed to simulate the performance of centrifugal chillers. The performance characteristics for flow capacity and efficiency of the centrifugal compressor are specified by coefficients for polynomial and bipolynomial functions of the Mach number of the impeller blade tips, the compressor head coefficient, and volumetric flow coefficient. Additional design-specific and geometrical parameters are needed to determine practical performance characteristics for a heat pump or chiller system. Ordinarily, many of the transport mechanisms involved in heat pump or chiller operations, design factors, and geometric constraints are parameterized as empirical correlations, some of which are design specific. To maintain the proper degree of accuracy of the simulations, these variables may have to be fine-tuned by a comparison between a set of computer simulation runs and the corresponding controlled experiments. Essentially, this process calibrates and validates the computer model.

Capacity Test Results

Capacity tests of a 125-ton (440-kW) centrifugal chiller were used to calibrate and validate the heat pump model. The chiller system has the following design specifications.

1. R-114 working fluid.
2. 125-ton (440-kW) cooling load at design point.
3. 88 F (31°C) condenser water inlet temperature.
4. 500-gal/min (31.5-L/s) condenser water flow rate.
5. 44 F (6.7°C) evaporator water exit temperature.
6. 450-gal/min (28.4-L/s) evaporator water flow rate.
7. Hot-gas bypass used below 95 tons (334 kW) of cooling.
8. Condenser tubes: 26-fin/in (1.02-fin/mm) fin spacing, 3/4-in (19-mm) OD, 90/10 CuNi, 8-ft (2.4-m) length, 123 tubes per pass, and 2 water-side passes.
9. Evaporator tubes same as condenser tubes except copper tube material.
10. No subcooling or evaporator superheat.
11. Motor heat rejection to the liquid line.

Numerous computer runs corresponding to the capacity test were made to calibrate the simulation results. Correction factors were calculated and applied to each of four variables as follows: isentropic efficiency -- 0.96, hot-gas bypass flow coefficient -- 1.5, condensing heat transfer coefficient -- 0.50, and evaporating heat transfer coefficient -- 0.83. A comparison of the calibrated results with the capacity test results is shown in Figure 3.

Each of the four variables was multiplied by its corresponding correction factor by all the simulations presented in this paper. Since all of the cases were variations of the same heat pump system, any conclusions reached from comparisons of results should be valid regardless of any inaccuracies in the correction factors.

PARAMETRIC STUDY

The calibrated heat pump model was used to analyze the performance of an existing 125-ton (440-kW) centrifugal chiller system at various operating and design-modification conditions. The simulation results of (1) a baseline case, (2) a modified baseline (MB) case with a slightly higher condenser water flow rate, (3) three design-component-variation cases, and (4) four different variable-speed centrifugal compressor cases are presented below.

Simulation of the Baseline Case

The designated 125-ton baseline case is specified only for the purpose of conducting the parametric analysis. Three additional conditions are imposed.

1. Condenser water flow rate is constant at maximum value, 500 gal/min (31.5 L/s), only when the condensing temperature is >90 F (32°C).
2. Condensing temperature is ≥ 90 F (32°C).
3. If the condensing temperature is 90 F (32°C), the condenser water flow rate is reduced to obtain an energy balance at that condition [i.e., condenser water flow rate is held at a fixed design value unless it must be reduced to keep the condensing temperature from falling below 90 F (32°C)].

Runs of the baseline case were made at condenser water inlet temperatures (CWTI) of 88, 85, 80, 75, and 70 F (31, 29, 27, 24 and 21°C).

Resulting curves for the baseline case are shown in Figure 4. Compressor power consumption decreases with decreasing cooling load in all cases, with a power surge occurring at 95 tons (334 kW) where the hot-gas bypass kicks on. Power also decreases with CWTI until the condensing temperature drops to 90 F (32°C), at which point the condenser water flow rate is adjusted to maintain the 90 F (32°C) condensing temperature. Note that when the condensing temperature is 90 F (32°C), the compressor power becomes independent of CWTI because the power is dependent on the refrigerant-side conditions only and the water flow is varied with CWTI to maintain constant refrigerant-side conditions.

A Modified Baseline Case

The designated modified baseline (MB) case is like the 125-ton (440 kW) capacity test design except that the condensing temperature constraint was removed and a higher condenser water flow rate of 636 gal/min (40.1 L/s) was fixed for all condensing temperatures. The higher condenser water flow rate resulted in about a 1% reduction in power consumption when compared with the simulation of the capacity test conditions.

Figure 5 shows simulations of the MB case made at CWTI values of 88, 70, 55, 35, and 28 F (31, 21, 13, 1.7 and -2.2°C). As in the original baseline case, power decreases with load at a given value of CWTI. Also, there is a power surge at 95 tons (334 kW) at the hot-gas bypass point. It is noted that removal of the 90 F (32°C) condensing temperature constraint allows for power savings at the lower condenser water temperatures.

Design Component Variations

Design component variations were made on the MB case to show the effects of adding more effective components to the system. Case MB-1 is similar to the MB case except that hot-gas bypass is used only when necessary to prevent compressor stalling, which will occur if the refrigerant flow rate becomes too small, instead of the 95-ton (334 kW) load criteria. Cases MB-2, MB-3, and MB-4 represent cumulative improvements over case MB, as a new improvement is added in each subsequent case, starting from the MB case. These improvements are defined as follows.

- For MB-2, the 26-fin/in (1.02-fin/mm) condenser tubes are replaced by 40-fin/in (1.57-fin/mm) tubes.
- For MB-3, the 26-fin/in (1.02-fin/mm) evaporator tubes are replaced by tubes with an enhanced coating to increase the boiling heat transfer.
- For MB-4, the original compressor motor is replaced by a high-efficiency motor.

Performance curves of case MB-1 are shown in Figure 6. Cases MB-2 through MB-4 appear similar to case MB except that the input power for each case is slightly lower than the previous case, respectively, with greater differences at large cooling loads and negligible differences at minimum load. Table 1 presents results for cases MB, MB-2, MB-3, and MB-4 for

comparison. Figure 6 shows a large range of part-load conditions in case MB-1, above 40 tons (140 kW), where the hot-gas bypass was unnecessary to prevent compressor stalling. A significant amount of energy could be saved if the bypass could be controlled to come on only when stalling is likely and not before. The predicted performance curve for case MB-2 resulted in a 3.8% improvement in power consumption over that of the MB case at the design point of 125-ton (440-kW) load and 88 F (31°C) CWTI. However, at part-load and lower values of CWTI, the improvement was significantly smaller. The predicted performance for case MB-3 resulted in a large reduction in power, 3% to 8%, over all values from 50% to 100% load. However, as the load dropped to 20%, the enhanced tubes in the evaporator required more power than the 26-fin/in (1.02-fin/mm) finned tubing. Case MB-4 yielded a 5% reduction in power at full-load and 88 F (31°C) CWTI and almost no reduction at 50% load and 70 F (24°C) CWTI. Below 50% load and 70 F (23°C) CWTI, the high-efficiency motor became less efficient than the original motor because its performance drops off rapidly when the power required is small.

All of the design-component improvements were not very effective at conditions where power consumption was small but became far more effective when power requirements were high.

Variable-Speed Cases

In the variable-speed centrifugal chiller simulations, the compressor speed was reduced as the CWTI decreased. This lower speed resulted in greater isentropic efficiency because the compressor was operating closer to full-load conditions. This was accomplished by reducing the speed, ϕ , and subsequently, the Mach number, M , in Equation 6 until the mass flow rate at full capacity, m_F (Equation 2), equaled the required mass flow rate, m_R (Equation 1).

Four different operating strategies for a variable-speed centrifugal chiller were simulated. The conditions of these cases are as follows.

Case V-1. A 125-ton (440-kW) design (nominal compressor speed - 12,000 rpm), running at the minimum speed required to meet the 100% capacity at different values of CWTI, with hot-gas bypass only when needed to prevent stalling [at 40-ton (141-kW) load].

Case V-2. A 125-ton (440-kW) design, running at 2.5% higher speed than Case V-1 to avoid stall lines altogether, thus eliminating any need for hot-gas bypass.

Case V-3. Similar to Case V-1 except that hot-gas bypass is turned on below 95-ton (334-kW) load.

Case V-4. Similar to Case V-1 except that hot-gas bypass is turned on at stall lines on compressor map, which vary with each value of CWTI, but is never turned on if the load exceeds 95 tons (334 kW) (this case is designated as modulated hot-gas bypass).

All four cases were run at 95, 85, 75, and 55 F (35, 29, 24, and 13°C) CWTI. Cases V-1, V-3, and V-4 were also run at 35 and 28 F (1.7 and -2.2°C) CWTI. Performance curves for case V-1 are shown in Figure 7. A graph of compressor speed vs CWTI is presented in Figure 8. In this plot, the compressor speeds for each value of CWTI for cases V-1, V-3, and V-4 are the same, but 2.5% higher for case V-2. Performance curves for cases V-2, V-3, and V-4 are shown in Figures 9 through 11, respectively.

In these variable-speed runs, the additional power losses caused by speed modulation are not included; therefore, the power consumptions shown in the curves are shaft power plus the loss due to motor inefficiency.

Comparison of case V-2 with case V-1 shows an increase in input power, due to the lower compressor efficiency at the higher speed, except when the load is below 37.5 tons (132 kW) and the hot-gas bypass is on, causing a greater power loss in case V-1. Case V-3 shows greater power input than case V-1 by increasing the range of cooling loads where the hot-gas bypass is on from 37.5 to 95 tons (132 to 334 kW). The power usage outside that range is unchanged. Case V-4, like case V-3, has greater power input than case V-1 over a range of cooling loads where the hot-gas bypass was on. However, this range was smaller than that in case V-3, yielding a slight performance improvement over case V-3. All of the variable speed cases showed improvement over the single-speed cases due to compressor efficiency improvements at lower compressor speeds.

ANNUAL PERFORMANCE COMPARISON

For a given annual cooling load profile with ambient air and seawater temperatures, the annual coefficient of performance (COP) values of a centrifugal chiller for each of the cases simulated were calculated based on the performance curves. The annual cooling load profile and ambient conditions are shown in Table 2 and the annual COP for the centrifugal chiller cases in Table 3.

It can be seen from Table 3 that case V-1, a variable-speed case with hot-gas bypass only on demand, results in the most energy-efficient operating strategy among the ten cases studied. The annual performance measured in COP of case V-1 is nearly twice that of the baseline case.

SUMMARY

A centrifugal chiller computer model was developed based on thermodynamic principles and empirical correlations. The correlations used were not necessarily derived under similar operating conditions. Calibrations of the model were made with respect to available capacity test data. The performance of a centrifugal chiller at various conditions and design modifications was predicted using the calibrated model. Cross comparisons among different case predictions were made. While the absolute performance away from calibrated points may be subject to error, the relative ranking among different cases will nevertheless hold. Through the parametric study, the performance of a centrifugal chiller was found to be improved substantially by using new component technology, compressor speed modulation, and different operating strategies. The most significant improvement in performance was obtained by modulating the compressor speed and using the hot-gas bypass only when necessary. These two improvements increased the annual COP more than the combined effects of improved heat exchanger components and a more efficient motor in the single-speed cases. More accurate transport process correlations and computer models should prove useful in the design, development and operation of more energy-efficient centrifugal chillers.

REFERENCES

- Beatty, K. O., Jr.; and Katz, D. L. 1948. "Condensation of vapors on outside of finned tubes," *Chem. Eng. Prog.*, January, pp. 55-68.
- Domanski, P.; and Didion, D. A. 1983. *Computer modeling of the vapor compression cycle with constant flow area expansion device*, NBS BSS 155, Washington, D.C.: National Bureau of Standards.
- Downing, R. C. 1974. "Refrigerant equations," *ASHRAE Transactions*, Vol. 80, Part II.
- Ellison, R. D.; and Creswick, F. A. 1978. *A computer simulation of steady state performance of air-to-air heat pumps*, ORNL/CON-16, Oak Ridge, TN: Oak Ridge Natl. Lab.
- Fischer, S. K.; and Rice, C. K. 1983. *The Oak Ridge heat pump models: I. a steady-state computer design model for air-to-air heat pumps*, ORNL/CON-81/R1, Oak Ridge, TN: Oak Ridge Natl. Lab.
- Flower, J. E. 1978. *Analytical modeling of heat pump units as a design aid and for performance prediction*, UCRL-52618, Livermore, CA: Lawrence Livermore Lab.

Freeman, T. L.; Beckman, W. A.; Mitchell, J. W.; and Duffie, J. A. 1975. *Computer modeling of heat pumps and the simulation of solar-heat pump systems*, ASME paper 75-WA/Sol-3, New York: American Society of Mechanical Engineers.

General Electric Company. 1971. "Forced convection, surface-roughness effects in ducts," *Heat Transfer Data Book*, Section 503.7, January, pp. 4-5.

General Electric Company. 1973. "Forced convection, liquids in smooth straight ducts," *Heat Transfer Data Book*, Section 503.3, p. 6.

Hiller, C. C.; and Glicksman, L. R. 1976. *Improving heat pump performance via compressor capacity control -- analysis and test*, Report 24525-96, Heat Transfer Laboratory, Cambridge, MA: Massachusetts Institute of Technology.

Hwang, B. C.; Wu, C.; Jackson, W. L.; and Chen, F. C. 1986. "Modeling and simulation of a naval shipboard heat pump," *International Journal of Modeling and Simulation*, June.

Oliver, P. P.; Sepsy, C. F.; and Jones, C. D. 1973. *A Thermodynamic computer simulation of an air-to-air heat pump system for a commercial building*, NSF-RA-N-73-375, National Science Foundation, November.

Rice, C. K.; Fischer, S. K.; Jackson, W. L.; and Ellison, R. D. 1981. *Design optimization and the limits of steady-state heating efficiency for conventional single-speed air-source heat pumps*, ORNL/CON-63, Oak Ridge, TN: Oak Ridge Natl. Lab.

TRW, Inc. 1982. *RD&D opportunities for large air conditioning and heat pump systems*, final report, ORNL/Sub/80-13817/1&20, June.

ACKNOWLEDGMENTS

This research was sponsored by David Taylor Naval Ship R&D Center, U.S. Navy, through the U.S. Department of Energy under contract DE-AC05-84OR21400 with Martin Marietta Energy Systems, Inc.

TABLE 1

Compressor Power vs. Cooling Load and CWTI for Cases MB, MB-2, MB-3, and MB-4

CASE	CWTI, F (°C)	Cooling load, tons (kW)				
		25 (88)	62 (220)	94 (331)	95 (334)	125 (440)
		Compressor power, kW				
MB	88 (31)	49.2	80.3	113.4	89.7	126.9
	70 (21)	37.4	59.0	81.3	68.3	92.6
	55 (13)	32.0	45.5	63.5	55.4	75.0
	35 (1.7)			35.6	33.3	50.3
	28 (-2.2)					36.6
MB-2	88 (31)	49.0	79.1	110.1	87.7	122.1
	70 (21)	37.3	58.3	79.8	67.3	90.3
	55 (13)	31.9	45.0	62.2	54.5	73.3
MB-3	88 (31)	48.4	76.4	103.5	83.1	112.1
	70 (21)	37.5	56.8	76.6	64.9	85.6
	55 (13)	32.7	43.4	58.6	51.8	69.1
MB-4	88 (31)	49.0	74.6	98.9	80.8	106.5
	70 (21)	38.6	56.6	74.9	64.1	83.0
	55 (13)	33.9	44.2	58.3	52.1	68.0

TABLE 2

Ambient Conditions and Annual Cooling Load Profiles

Ambient air temp. range, F (°C)	Ambient water temp., F (°C)	Operation time, h	Number of machines	AC load per machine, tons (kW)
<u>Operating condition A</u>				
10 to 30 (-12 to -1)	55 (13)	1122	1	78 (275)
30 to 38 (-1 to 4)	55 (13)	438	1	100 (352)
38 to 64 (4 to 18)	55 (13)	1396	2	62 (220)
64 to 90 (18 to 32)	72 (22)	1424	2	82 (290)
<u>Operating condition B</u>				
10 to 30 (-12 to -1)	55 (13)	219	4	48 (169)
30 to 50 (-1 to 10)	55 (13)	219	4	56 (197)
50 to 70 (10 to 21)	55 (13)	219	4	64 (226)
70 to 90 (21 to 32)	75 (24)	219	4	72 (255)
<u>Operating condition C</u>				
10 to 26 (-12 to -3)	55 (13)	723	3	101 (356)
26 to 62 (-3 to 17)	55 (13)	1544	4	87 (308)
62 to 90 (17 to 32)	71 (22)	1237	4	100 (352)
Total		8760		

TABLE 3

Annual Performance Comparison
Among Cases

Cases*	Annual COP
Baseline	3.64
MB	4.79
MB-1	5.25
MB-2	4.88
MB-3	5.10
MB-4	5.12
V-1	7.06
V-2	6.84
V-3	6.17
V-4	6.30

*Defined in previous sections.

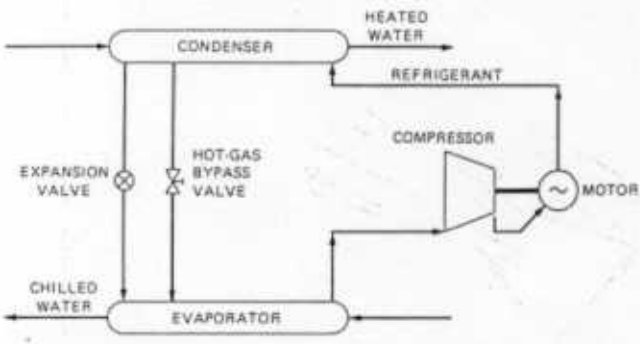


Figure 1. Schematic of a basic heat pump system

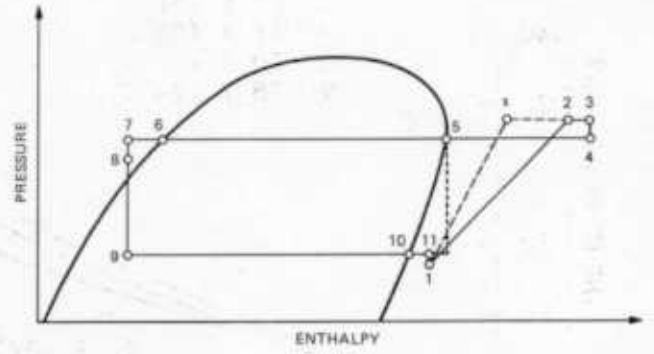


Figure 2. The basic thermodynamic cycle

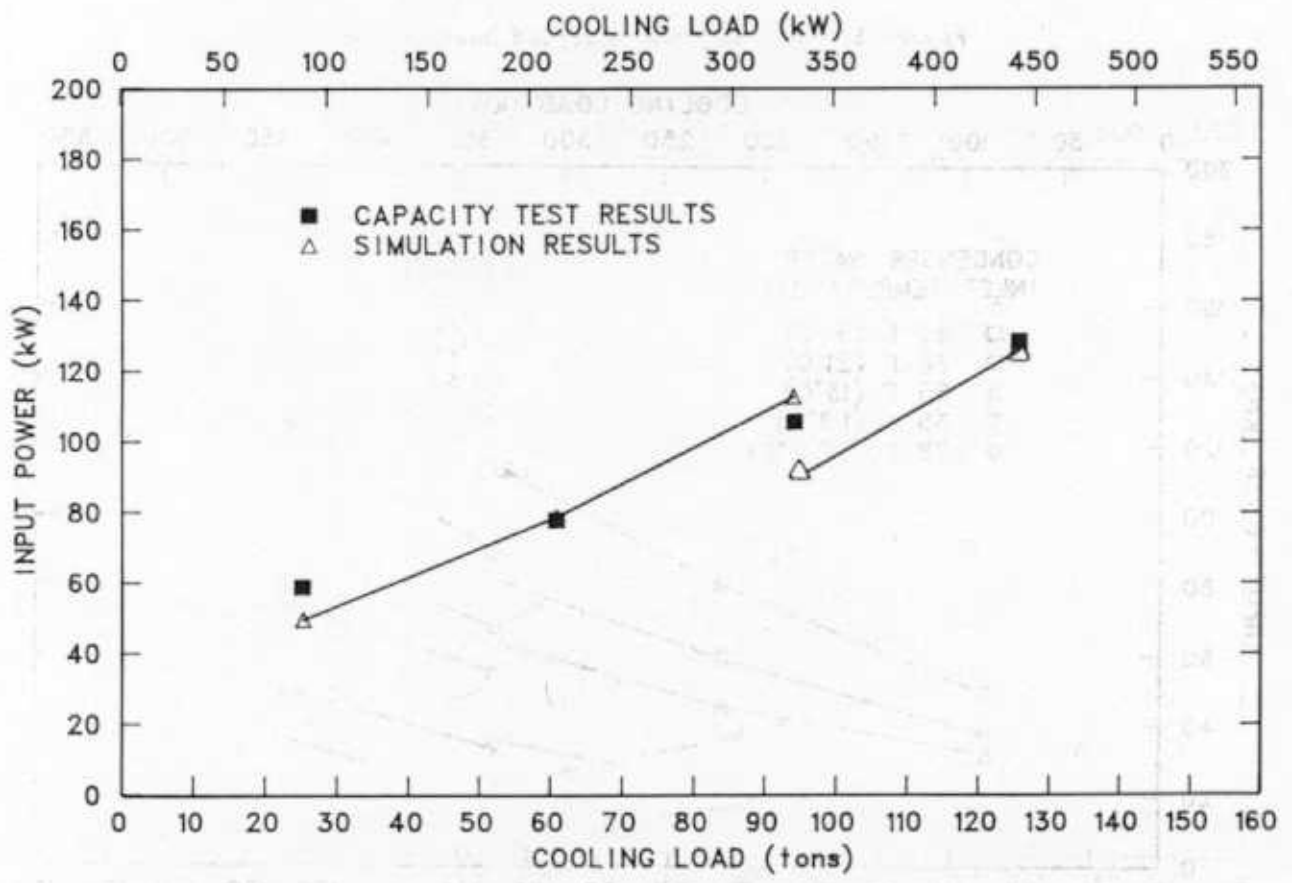


Figure 3. Comparison of the capacity test results with the simulation

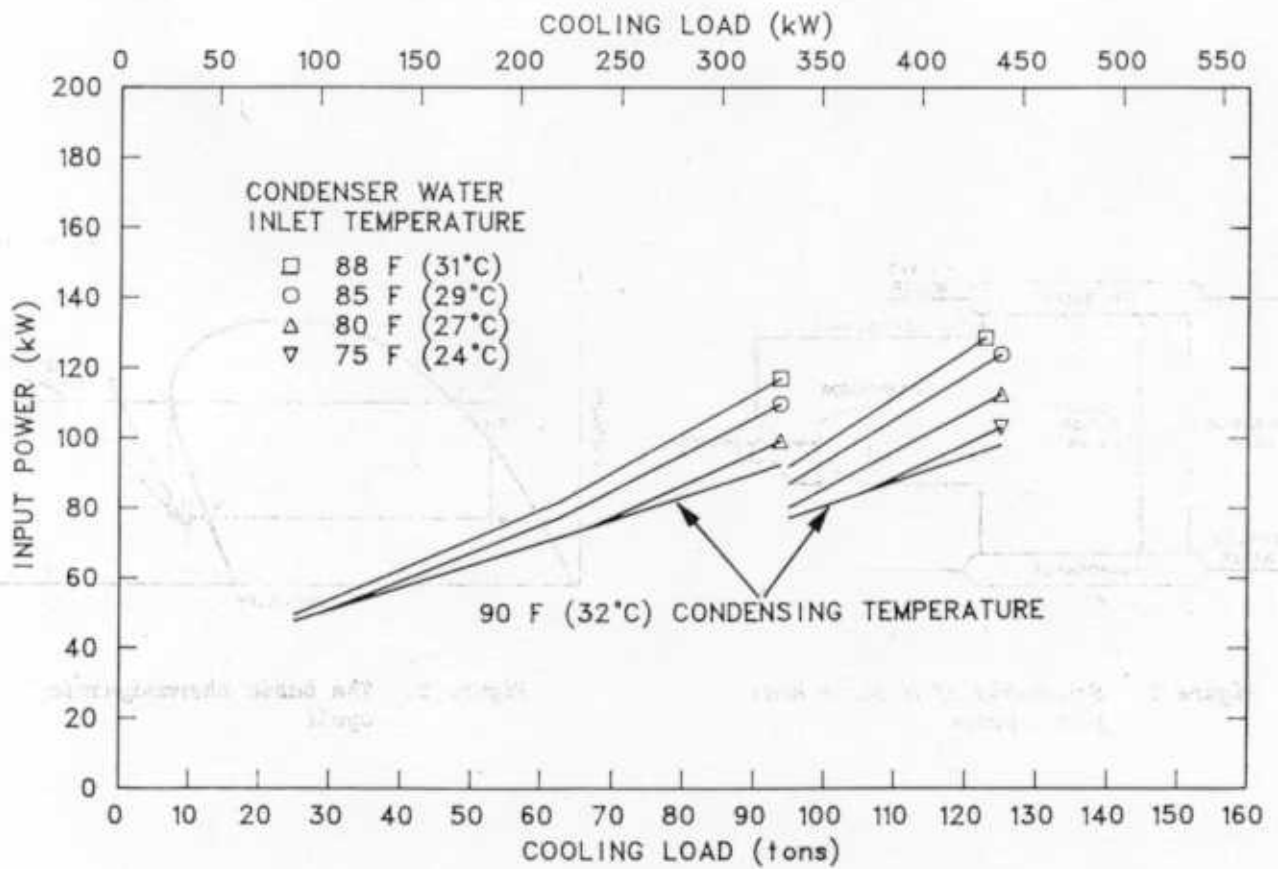


Figure 5. Case MB, the modified baseline case

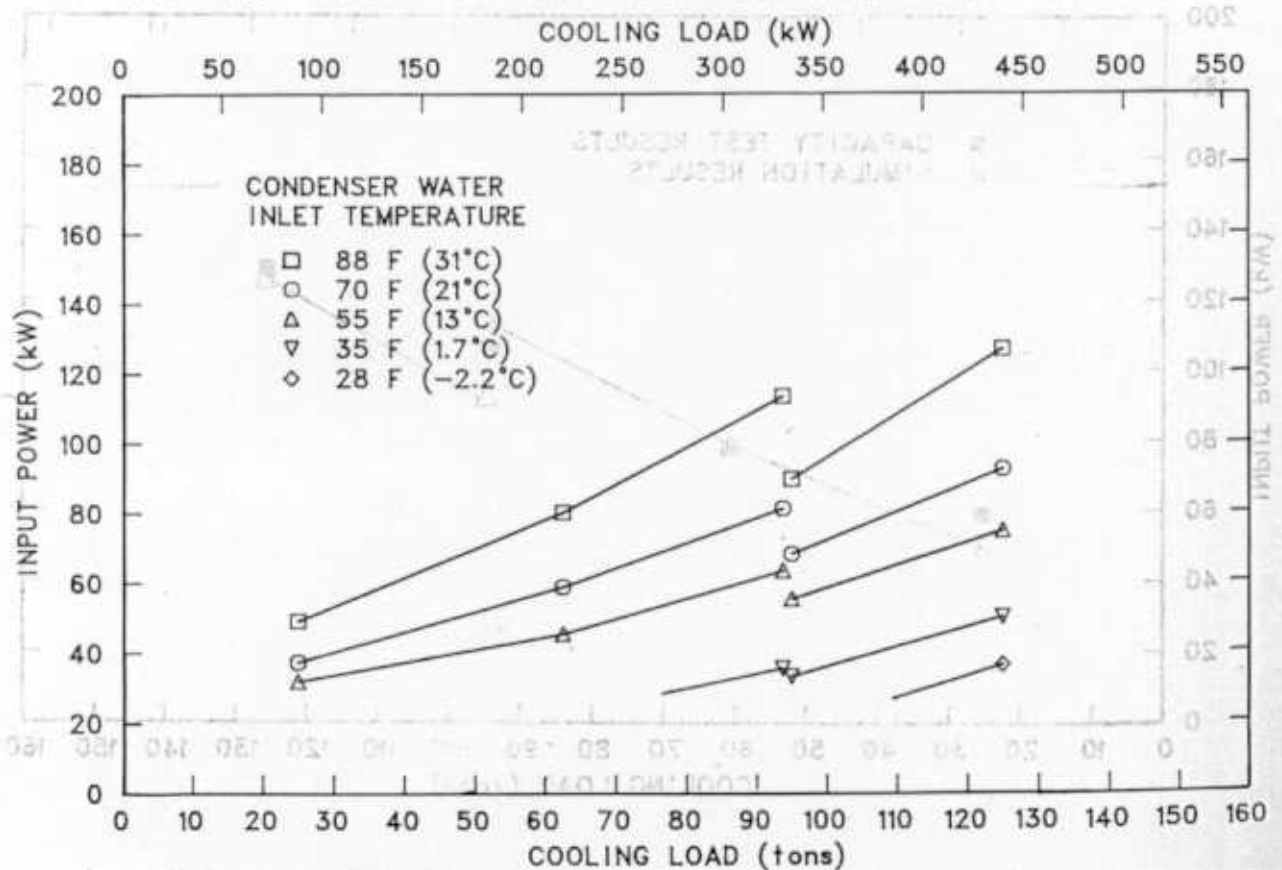


Figure 4. The Baseline case, condensing temperature not less than 90 F

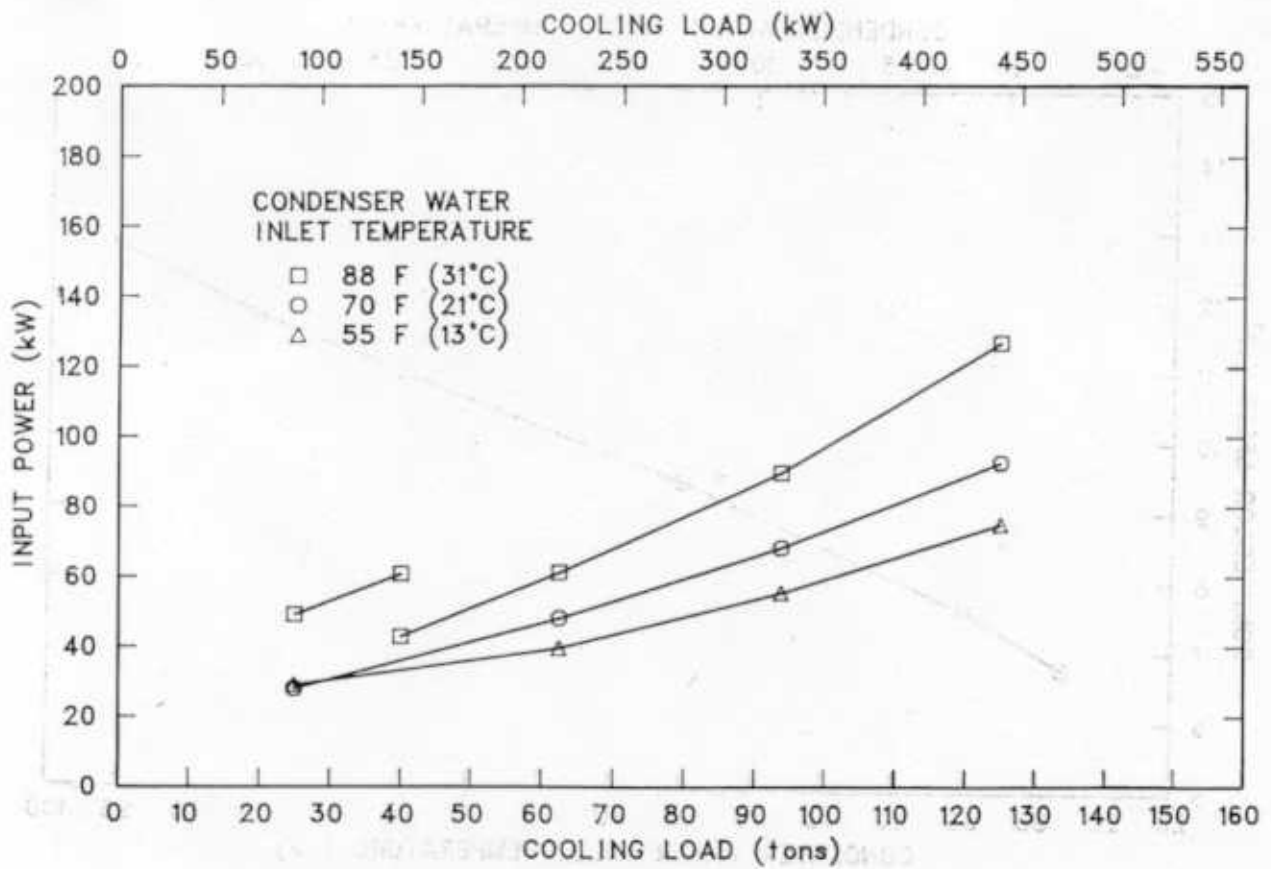


Figure 6. Case MB-1, hot gas bypass used only when needed

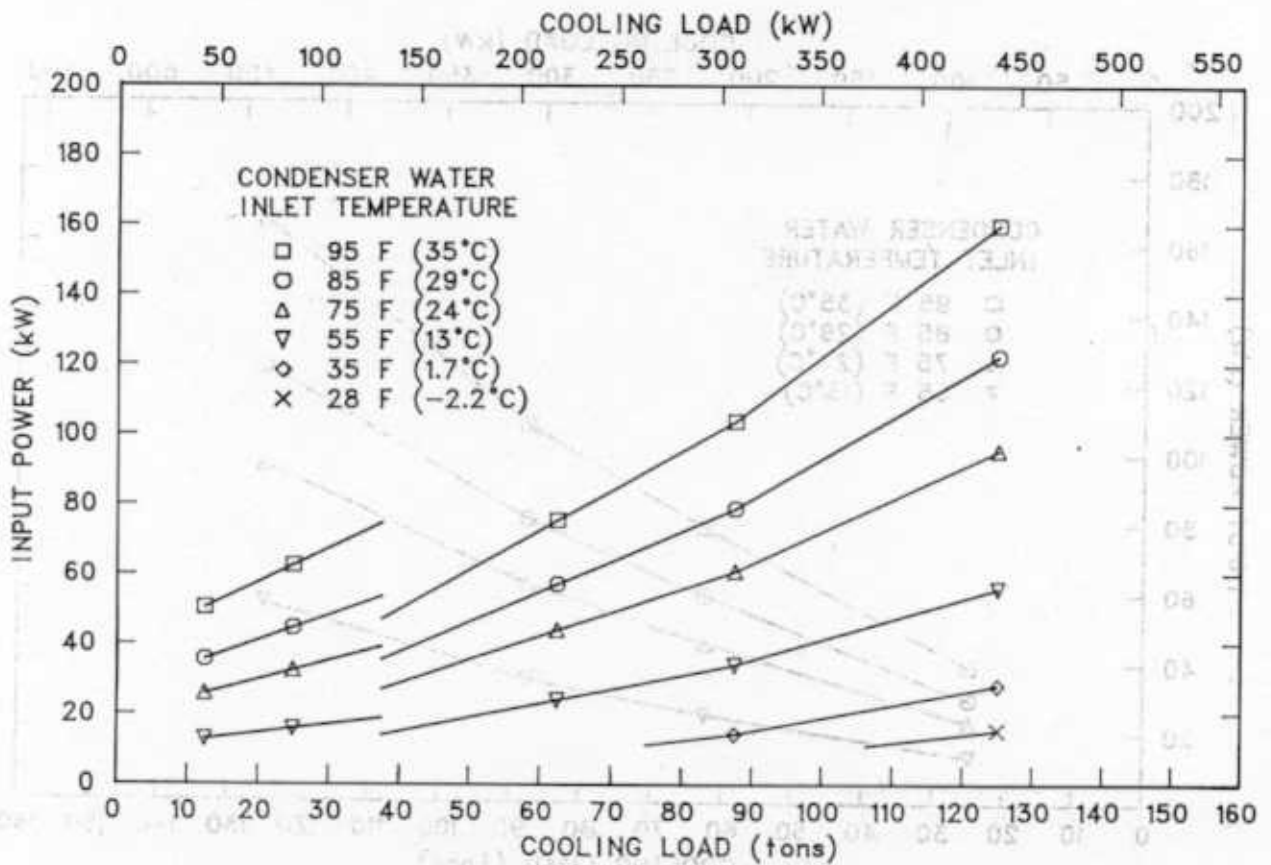


Figure 7. Variable-speed case V-1

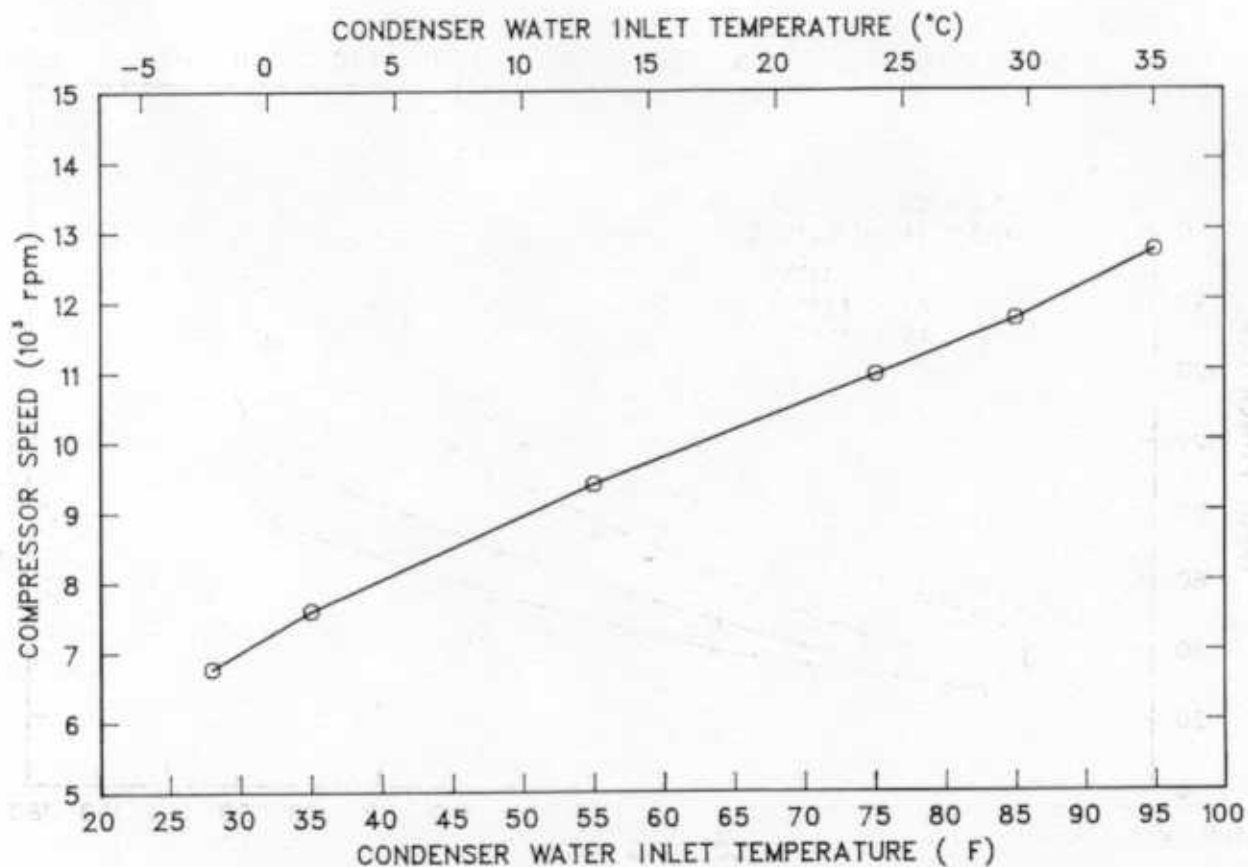


Figure 8. Speed versus CWTI for variable-speed cases

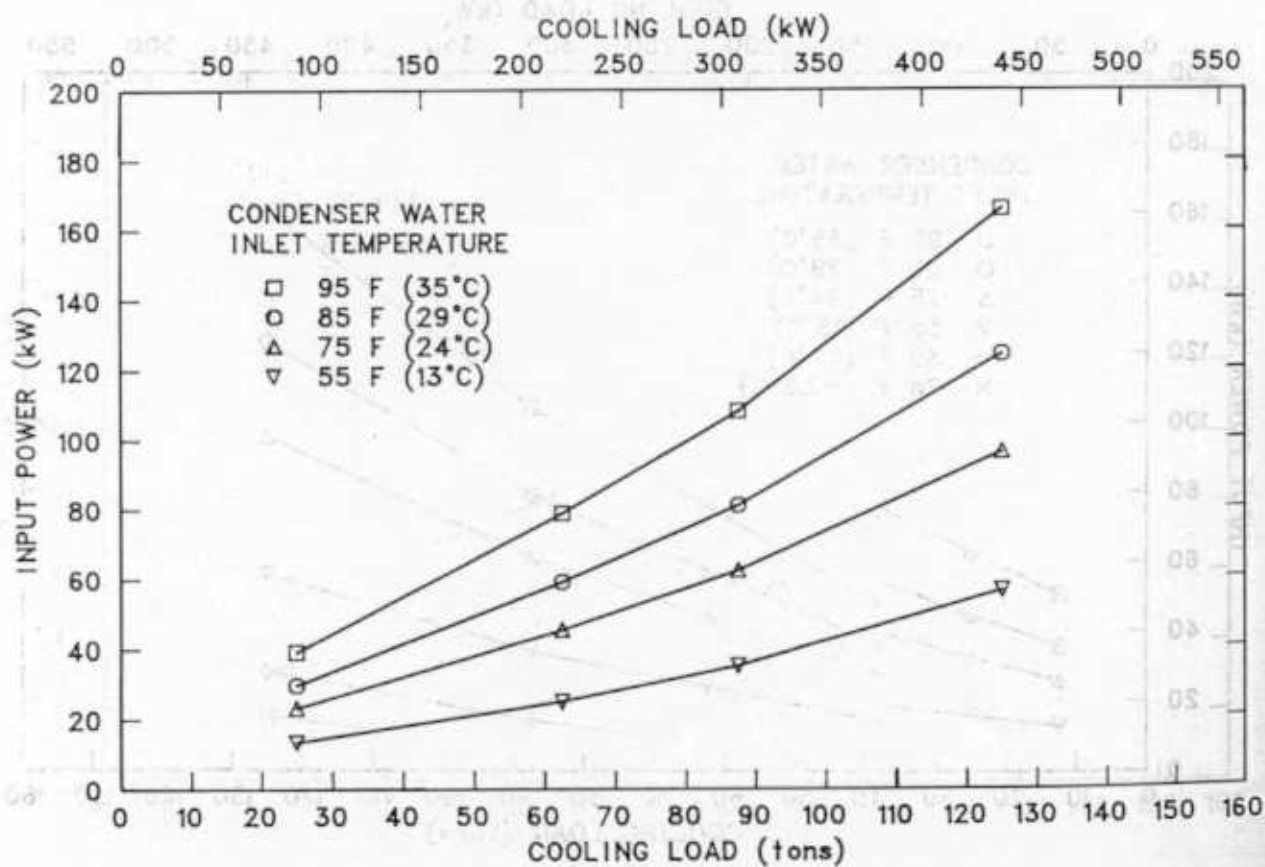


Figure 9. Variable-speed case ψ -2.

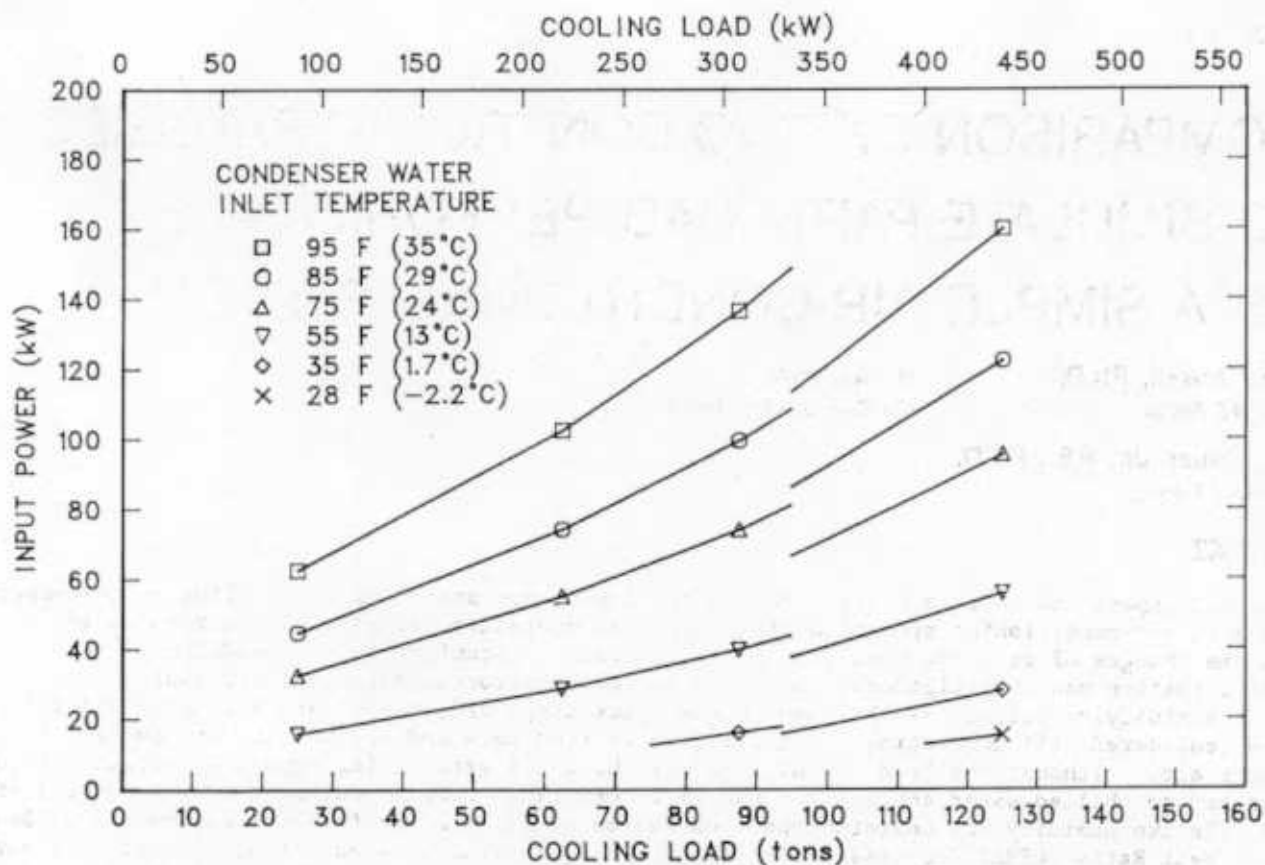


Figure 10. Variable-speed case V-3

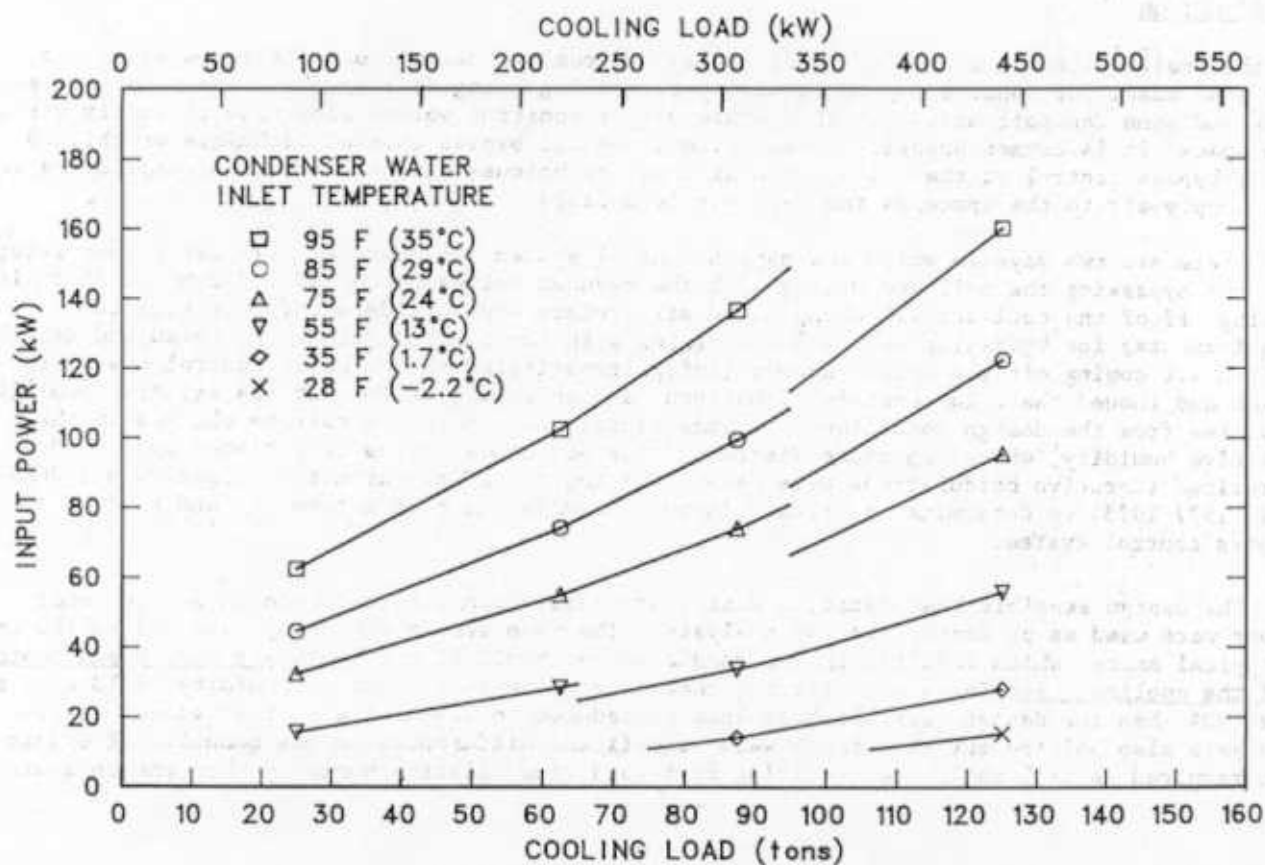


Figure 11. Variable-speed case V-4